Numerical study on the transient behavior of a radial pump during starting time

Faouzi Omri, Lamjed Hadj Taieb and Sami Elaoud

ABSTRACT

This paper presents a fast simulation model for predicting the dynamic response of a motor-pump system to startup event. The purpose is to analyze the effect of the impeller acceleration time, the final flow rate and the impeller geometry on the pump transient flow during starting operations. The motor speed and torque variations were predicted by simulating the transient law of the three-phase induction motor by adopting the d-q axes theory. The pump model was built by solving the unsteady flow governing equations with the method of characteristics (MOC). The whole model was validated with available tests from literature. Accordingly, the computation of impeller acceleration, the motor torque, the unsteady pressure and flow rate was made for various starting conditions. The results have revealed that during its starting time, the pump hydraulic transients are well influenced by the motor speed acceleration, the flow inertia and the impeller geometry. Through the analysis of the simulation results, the conclusion was that the accuracy of the present method is reasonable, and it can be used for assisting pumping system design.

Key words | d-q axes theory, impeller geometry, induction motor, method of characteristics, radial pump, transient flow

Faouzi Omri (corresponding author)
Lamjed Hadj Taieb
Sami Elaoud
Laboratory of Applied Fluid Mechanics, Process
  Engineering and Environment,
National School of Engineering of Sfax,
3038 Sfax,
Tunisia
E-mail: *omrifawzi@yahoo.fr*

Lamjed Hadj Taieb
College of Engineering, Department of Mechanical
  Engineering,
Prince Sattam bin Abdulaziz University,
16273, AlKharj,
Saudi Arabia

HIGHLIGHTS

- Radial pump startup transient was investigated using the method of characteristics (MOC).
- Pump fast startup can cause a significant head impact and high torque oscillations.
- Startup hydraulic transients are well influenced by the motor acceleration time and the impeller geometry.

INTRODUCTION

Water distribution networks (WDNs) represent one of the largest infrastructure assets of an industrial society (Darweesh 2018). Their security and efficiency are of paramount importance to human health and economic development (Duan *et al.* 2020). The leading causes behind hydraulic network anomalies may be essentially associated with leakage, corrosion, deformation, and hydraulic transients. Centrifugal pumps are the most commonly used devices for pressure generation and fluid transmission in water systems. The variation of their operating conditions such as startups, shutdown or rapid changes in control valve settings will lead to transient flow disturbances which are closely related to the safety and reliability of the WDNs (Yang *et al.* 2015; Triki 2018).

During the past few decades, there have been numerous studies on centrifugal pump startup characteristics. Saito (1982) experimentally and theoretically explored the transient characteristics of a diffuser pump during starting time. His results have clearly shown the significant differences between pump startup transients and the steady state performances. In addition, his conclusion was that the response of a centrifugal pump to startup events is influenced by three important factors which are the mass of water in the pipes, the downstream valve openings and the starting time. On a similar subject, a theoretical and experimental study was made by Tsukamoto & Ohashi (1982). As a result of this study, they demonstrated that the impulsive pressure and the lag in circulation formation around the impeller vanes are the main reasons for the difference between the dynamic and quasi-steady characteristics of the turbo pump during the starting period. For the purpose of predicting the dynamic behavior of a centrifugal pump during operating transients, Thanapandi & Prasad (1994, 1995) developed a numerical model using the method of characteristics (MOC). The numerical results were validated with experiments and the conclusion was that the change of the pump behavior during normal startup and stopping is quasi-steady. They also deduced that the quasi-steady model can be used to predict the pump transient characteristics where the impeller acceleration is small. Farhadi *et al.* (2007) theoretically studied transient pump startup in the primary cooling system of a nuclear reactor. They investigated the effect of the moment of inertia on the pump flow rate during starting time. It has been found that for a pumping system with a high moment of inertia, the fluid flow is established gradually and it requires more time to reach its final value. However, for a pump having a small moment of inertia the steady-state operating flow will be approached much more rapidly. To investigate the mechanism of pump startup transients, Wu *et al.* (2009) established a three-dimensional model for simulating the unsteady flow in a centrifugal pump during the starting period. The pump transient performances were analyzed when the impeller started from stationary to maximum speed, and the effects of different pipeline resistances were also evaluated.

In recent years, Duplaa *et al.* (2010) experimentally tested a centrifugal pump fast startup in cavitating and non-cavitating conditions. They found that at high flow rate, large scale low-frequency oscillations are obtained on the pressure signal at the delivery, whereas at a lower flow rate, only a drop at the end of startup is detected. They also reported, according to the numerical study presented in Dazin *et al.* (2007), that centrifugal pump fast startup results in severe transient effects that are mainly governed by the speed acceleration and the flow rate increase.

Transient flows in a centrifugal pump during its starting period were also experimentally and numerically investigated by Li *et al.* (2011). They used the two-dimensional particle image velocimetry technique (PIV) to capture the transient flow evolutions in the pump's diffuser. They also established a three-dimensional model with a dynamic slip region (DSR) method to simulate the transient flow evolutions during startup operations. The conclusion was that in the early stage of the startup, the transient vortex evolution between blades is the main reason leading to the transient head coefficient being lower than the steady state value. Based on the experimental data of performance curves, Wan & Huang (2011) established an inversion model to obtain the performance curves of a centrifugal pump. The proposed method is adopted for hydraulic transient simulation of centrifugal pump failure and startup. Meanwhile, the MOC numerical model was applied to compute the gradually unsteady process with different hydraulic pressure. It was found that the inversion method can give more reasonable results to describe the pump's transient process and it can be used as an effective tool to achieve the complete characteristic curves of pumps.

Lucius & Brenner (2011) presented a numerical method to investigate the effect of the rotating stall on the internal flow field of a centrifugal pump. The paper describes how the fluctuations of fluid properties during rotating stall can be investigated in order to determine their importance for the excitation of structural vibrations. As a conclusion, they found that the data analysis in relative frame can deliver major excitation frequencies not visible in stationary frame analysis. The numerical method was also successfully applied in pump startup simulations by Elaoud & Hadj-Taïeb (2011), Chalghoum *et al.* (2016) and others. They have proposed various models by solving the unsteady flow governing equations with the 1D method.

More recently, Page *et al.* (2019) proposed a pump speed controller to solve the pressure deficiency in water system distribution (WDS). As a function of the average pressure deviation, the controller adjusts the pump speed to supply the adequate pressure. Dutta *et al.* (2020) adopted a machine learning (ML) algorithm as a predictive control method for the identification of water hammer problems in a pumping system. It is an experiment-based work intended to discover the hydraulic anomalies through the analysis of the pump motor current signal. Duan *et al.* (2020) proposed an important comprehensive literature review of the hydraulic models for predicting and describing the transient flows that are commonly used for the effective design and management of urban water supply systems (UWSS). First, the review illustrates the importance of transient flow phenomena and its impact on the safety, reliability and availability of pipe systems. Thereafter, the authors discussed the advances and limitations of current transient models and methods, including the derivations of governing equations in 1D and 2D forms, unsteady friction, turbulence formulas, viscoelastic models and numerical simulation methods. On the other hand, the utilizations of transient flows for pipeline diagnosis and fault detection are reviewed. Four types of common pipe defects, namely leakage, discrete partial blockage, extended partial blockage, and unknown branch, are elaborated and evaluated. To control the water hummer processes in the water supply systems, Chen *et al.* (2021) proposed a solution for determining the size of the air tank in the actual operation process. The operating parameters of the air tank were optimized by introducing the influence of friction and the hydraulic impedance of the connecting pipes.

Despite various contributions, the unsteady flow phenomena in turbo pumps remains unclear, complex and difficult to investigate. In addition, the characteristic method (MOC) is not fully exploited in this field. The impeller speed, on the other hand, is often assumed to follow linear or exponential law. These approximations hide the natural fluctuations of the impeller velocity that occur at the very beginning of starting time.

At the outset, this paper presents a simple and fast numerical method applicable to radial pump startup analysis. The unsteady flow equations of continuity and motion are numerically solved with the 1D method of characteristics. To get the impeller speed variation, the induction motor is modeled with the d-q axis transformation theory. The proposed model is validated with experimental data presented in Duplaa *et al.* (2010). Thereafter, the numerical solution is used to investigate the influence of several parameters (e.g. the impeller acceleration time, the final flow rate, the impeller width, the impeller blade exit angle and the number of impeller vanes) on the unsteady flow during pump starting period. Through the interpretation of the instantaneous motor-pump performance; it is found that the impeller geometry, final flow rate and moment of inertia are the key parameters for predicting the hydrodynamic pump characteristics. Accordingly, this work proposes a new coherent model, including the centrifugal pump and its drive motor which can provide useful information regarding the electro-hydraulic transient regimes in a new pumping system.

METHODS AND MATERIALS

Modeling of 3-phase induction motor

The d-q model has been well tested and proven to be reliable and accurate for transient study of the induction motor (Lee *et al.* 1984). It is introduced herein to facilitate the pump motor analysis and reduce computation time (Orille *et al.* 1999). This method consists of transforming the motor equations in the stationary reference frame, from the real three phase axes to the rotating reference frame described by direct quadrature (d-q) transformation (Figure 1). In general, for any arbitrary value of θ, the transformation of the stator and the rotor variables from the three phases stationary coordinates (x_1, x_2, x_3) to the (d-q) rotating coordinates is carried out through Park's transformation described as follows (Krause *et al.* 2013):

$$\begin{bmatrix} x_d \\ x_q \end{bmatrix} = P(\theta) \begin{bmatrix} x_1 \\ x_2 \\ x_3 \end{bmatrix} \tag{1}$$

where:

$$P(\theta) = \sqrt{\frac{2}{3}} \begin{bmatrix} cos(\theta) & cos(\theta - 2\pi/3) & cos(\theta + 2\pi/3) \\ -sin(\theta) & -sin(\theta - 2\pi/3) & -sin(\theta + 2\pi/3) \end{bmatrix} \tag{2}$$
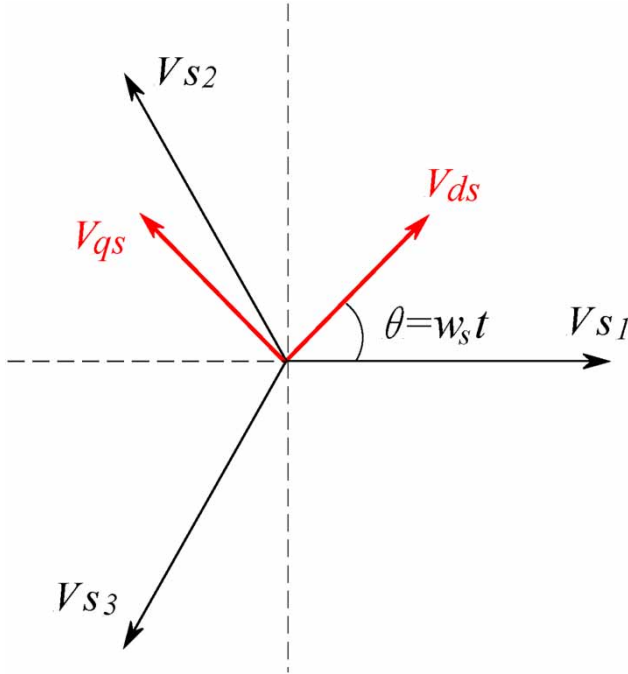
Figure 1 │ Voltage space vector in d-q plane.

The three phase voltages supplied to the induction motor in a stationary reference frame are given as:

$$\begin{bmatrix} v_{S1} \\ v_{S2} \\ v_{S3} \end{bmatrix} = \begin{bmatrix} V\sqrt{2}\cos(w_s t) \\ V\sqrt{2}\cos(w_s t - 2\pi/3) \\ V\sqrt{2}\cos(w_s t - 4\pi/3) \end{bmatrix} \tag{3}$$

in which t is time, $w_s = 2\pi f$ is the stator voltage pulsation, $V = 220\,v$ is the RMS (root mean square) value of voltage and $f = 50\,Hz$ is the frequency.

The stator voltage equations in the (d-q) plane are expressed as:

$$\begin{bmatrix} v_{ds} \\ v_{qs} \end{bmatrix} = P(\theta) \begin{bmatrix} v_{S1} \\ v_{S2} \\ v_{S3} \end{bmatrix} \tag{4}$$

In the rotating reference frame (d-q), the induction motor voltage equations for the stator and the rotor windings, after transformations, can be written as (Mimouni

et al. 2004):

$$\frac{di_{ds}}{dt} = \frac{1}{\delta L_s L_r}\left[L_r v_{ds} - L_r R_s i_{ds} + (L_s L_r - M^2 g)w_s i_{qs}\right.$$
$$\left. + MR_r i_{dr} + ML_r w_r i_{qr}\right]$$
$$\frac{di_{qs}}{dt} = \frac{1}{\delta L_s L_r}\left[L_r v_{qs} + (M^2 g - L_s L_r)wi_{ds} - L_r R_s i_{qs}\right.$$
$$\left. - L_r M w_r i_{dr} + MR_r i_{qr}\right]$$
$$\frac{di_{dr}}{dt} = \frac{1}{\delta L_s L_r}\left[-Mv_{ds} + MR_s i_{ds} - ML_s w_r i_{qs}\right.$$
$$\left. + L_r R_r i_{dr} + (L_s L_r g - M^2)wi_{qr}\right]$$
$$\frac{di_{dr}}{dt} = \frac{1}{\delta L_s L_r}\left[-Mv_{qs} - L_s M w_r i_{ds} + MR_s i_{ds}\right.$$
$$\left. + (M^2 - L_s L_r g)w_s i_{dr} - L_s R_r i_{qr}\right]$$
$$\frac{dg}{dt} = \frac{p}{Iw_s}[T_{em} - T_r] \tag{5}$$

where i_{ds}, i_{qs} are the stator direct-axis and quadrature axis currents (A); i_{dr}, i_{qr} are the rotor direct-axis and quadrature axis currents (A); R_s, R_r are the resistances of the stator and rotor (Ω); L_s, L_r are the cyclic inductances of the stator and rotor (H); M is the mutual cyclic stator-rotor inductance (H); δ is the magnetic leakage factor (–); g is the sliding coefficient (–); p is the motor pole number (–); I is the inertia of the rotating parts (kgm^2); w_s, w_r are the rotor and stator pulsation (rad/s); T_{em} is the motor electromagnetic torque (Nm); T_r is the load torque (Nm).

The Blondel dispersion factor δ is expressed as:

$$\delta = 1 - \frac{M^2}{L_S L_r} \tag{6}$$

The stator and rotor pulsation are given by:

$$w_r = (1 - g)\frac{w_S}{p}, \; w_S = \frac{d\theta}{dt} \tag{7}$$

The motor stator current is expressed as:

$$i_S = \sqrt{\frac{2}{3}}(i_{dS}\cos(w_S t) - i_{qS}\sin(w_S t)) \tag{8}$$

The electromagnetic torque equation is given as:

$$T_{em} = p \cdot M(i_{dr}i_{qs} - i_{qr}i_{ds}) \tag{9}$$

The numerical integration of the motor equations with the pump resistant torque expression that will be seen later allows the motor speed and the torque evolution to

be obtained. More information can be found in Okoro (2003) and Mimouni *et al.* (2004).

Equations of motion for coupled motor pump

During the starting time, the pump motor provides an initial torque T_f to overcome the friction of the fluid circulating in the system and the friction of the rotating parts. Reaching the steady state, no torque is needed for acceleration. Torque is needed only to overcome the frictional and hydraulic losses. Therefore, the governing equation for mechanical model can be expressed as follows (Elaoud & Hadj-Taïeb 2011):

$$(I_M + I_p)\frac{d\Omega}{dt} + T_f = T_{em} - T_r \tag{10}$$

In this equation I_M is the inertia of the motor, I_p is the inertia of the impeller including the rotating water inertia, Ω is the impeller angular velocity, T_{em} is the motor torque and T_r is the resistant hydrodynamic torque. This torque depends on the impeller angular speed and the flow rate Q (Elaoud & Hadj-Taïeb 2011):

$$T_r = k_1\Omega^2 + k_2\Omega Q - k_3 Q^2 \tag{11}$$

The hydrodynamic torque coefficients k_1, k_2 and k_3 are obtained from the pump steady state characteristic curves.

Model exit angle effect

The theoretical head developed by the impeller can be expressed by using the Euler equation with the blade output velocity (Figure 2) as:

$$H_i = \frac{U_2}{g}(U_2 - Q/Atg\beta_2) \tag{12}$$

where $U_2 = r_2\Omega^2$ denotes the impeller peripheral velocity, r_2 the outer impeller radius and β_2 is impeller blade exit angle.

The flow velocity at the exit of the impeller does not follow correctly the profile of the rotor blade. It presents an angular deflection, which depends on the blade
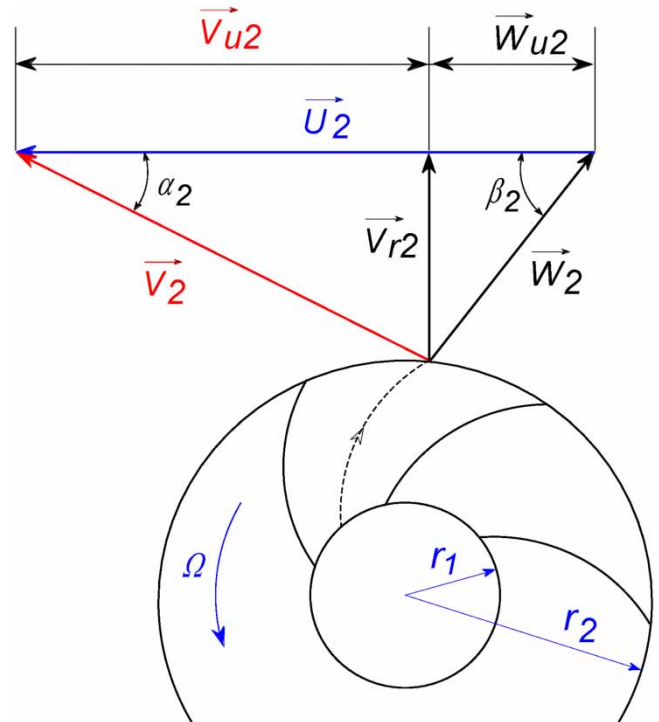

Figure 2 │ Outlet velocity diagram for the pump impeller.

number, the impeller exit angle, and the flow rate. A better explanation is presented in Figure 3, which shows the difference between the real (in blue) and theoretical (in red) triangles of the impeller output velocities. The slip factor is used to specify the flow effect at the exit of a centrifugal pump impeller. Several tests and correlations were analyzed to obtain formulas for the slip factor. In this study, the
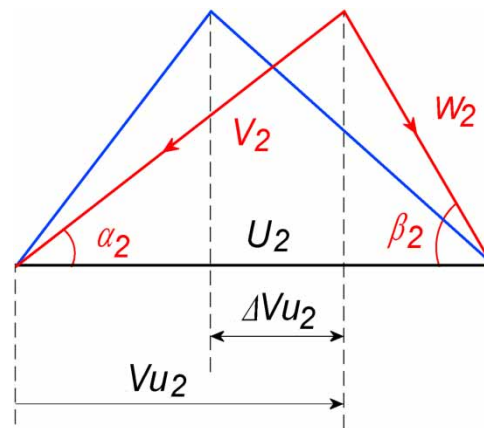

Figure 3 │ The impeller sliding effect in the outlet triangle velocity. Please refer to the online version of this paper to see this figure in color: http://dx.doi.org/10.2166/aqua.2021.136.

following correlation is used (Brennen 1994):

$$\sigma = \frac{U_2 - \Delta V_{u2}}{U_2} = 1 - \frac{\Delta V_{u2}}{U2} \tag{13}$$

where V_{u2} is the tangential component of the flow absolute velocity V_2.

The slip factor of a centrifugal pump impeller is frequently estimated by means of the empirical formula (Wiesner 1967):

$$\sigma = 1 - \frac{\sqrt{sin\beta 2}}{Z^{0.7}} \tag{14}$$

where Z is the number of impeller vanes.

As a result, the pump head is estimated by the following relation (Li 2011):

$$H = \sigma \frac{U_2}{g} (U_2 - Q/Atg\beta_2) \tag{15}$$

Hydraulic loss model

The hydraulic losses during the transient regime are supposed to be equal to those in steady operations. In this study all hydraulic losses are reduced to the impeller friction loss, the volute friction loss and the impeller shock loss. The impeller friction loss is defined as the linear loss caused at the wall boundary layer of the blade, and the flow of the whole channel can be equivalently simplified to Z (number of the impeller vanes) pipe flows. The head friction loss by unit of impeller passage length are expressed as (Bing *et al.* 2012):

$$h_{imp} = \lambda_{imp} Z \frac{Q|Q|}{2gD_{himp}A_{imp}^2} \tag{16}$$

where D_{himp} is the hydraulic diameter of the impeller passage section (A_{imp}), and λ_{imp} is the friction coefficient that depends on the Reynolds number and the surface roughness of the impeller passage.

At the impeller inlet, a shock circulation exists inside the pump eye when the flow discharge differs from that of

adapted flow rate Q_0. The corresponding head due to the impeller shock loss is given as (Matteo *et al.* 2019):

$$h_{shock} = k_S \frac{\Omega}{\Omega_N} \frac{(Q - Q_0)^2}{gD_{himp}A_{imp}^2} \tag{17}$$

In this equation Ω_N denotes the impeller nominal velocity. The shock loss coefficient k_s is obtained from the pump steady state performance curves.

The volute friction loss depends on the volute through flow velocity, the surface roughness of volute and the hydraulic diameter of the passage section. The head friction loss by unit of volute passage length is expressed as:

$$h_{vol} = \lambda_{vol} \frac{Q|Q|}{2gD_{hv}A_v^2} \tag{18}$$

where D_{hv} is the hydraulic diameter of the volute passage section (A_v), and λ_{vol} is the friction coefficient of the volute passage.

Pump modeling

Equations for unsteady flow through the impeller

The unsteady flow through the impeller vanes is assumed as a flow through rotating conduit with a diameter equivalent to the mean hydraulic diameter of the impeller passage. A similar mathematical approach has been used in Saidi & Daneshyar (1990), Thanapandi & Prasad (1995), and Chalghoum *et al.* (2016). The basic equations of continuity and motion, in a reference frame rotating with the impeller, after neglecting unimportant terms, can be expressed as:

$$\frac{\partial H}{\partial t} + \frac{a^2}{gA} \frac{\partial Q}{\partial x} = 0 \tag{19}$$

$$\frac{1}{A} \frac{\partial Q}{\partial t} + g \frac{\partial H}{\partial x} + \lambda \frac{Q|Q|}{2D_{himp}A_{imp}^2} - r\Omega^2 = 0 \tag{20}$$

where x is the space distance along the rotating passage, A_{imp} is the impeller passage section, $Q(x, t)$ is the fluid discharge, $H(x, t)$ is the pump head, a is the pressure wave speed, $D_{himp} = 4lb/2(l + b)$ is the hydraulic diameter of the

section A, b is the blade height, l is the blade length and Ω is the impeller angular velocity. The term $r\Omega^2$ in Equation (20) represents the centrifugal force developed by the rotating impeller.

Method of characteristics (MOC)

The method of characteristic (Wylie & Streeter 1978; Chaudhry 1979; Iffa & Triki 2019) consists of transforming the partial first order differential Equations (19) and (20) into a system of total differential equations integrated numerically along two characteristic lines C^+ and C^- (Figure 4). The ordinary equations obtained after

Figure 4 │ Characteristic lines in the *x-t* plane.

transformation are identified as:

$$C^+ \begin{cases} \dfrac{gA}{a}dH + dQ + JAgdt - r\Omega^2 A\,dt = 0 \\ dx = adt \end{cases} \qquad (21)$$

$$C^- \begin{cases} -\dfrac{gA}{a}dH + dQ + JAgdt - r\Omega^2 A\,dt = 0 \\ dx = -adt \end{cases} \qquad (22)$$

in which J is calculated from Equations (16) and (17) as:

$$J = h_{imp} + h_{shock} \qquad (23)$$

The flow inside the pump is calculated according to the 1D discretization approach. Figure 5 describes the schematics of the analytical model, in which the computation process is started with known steady state conditions, so that H and Q are known initial values at each sections of the grid along $t = 0$. The integration of Equations (21) and (22) along the $i + 1$ characteristic lines can be written in
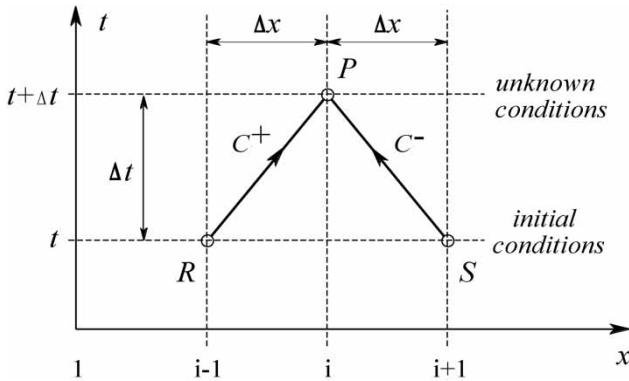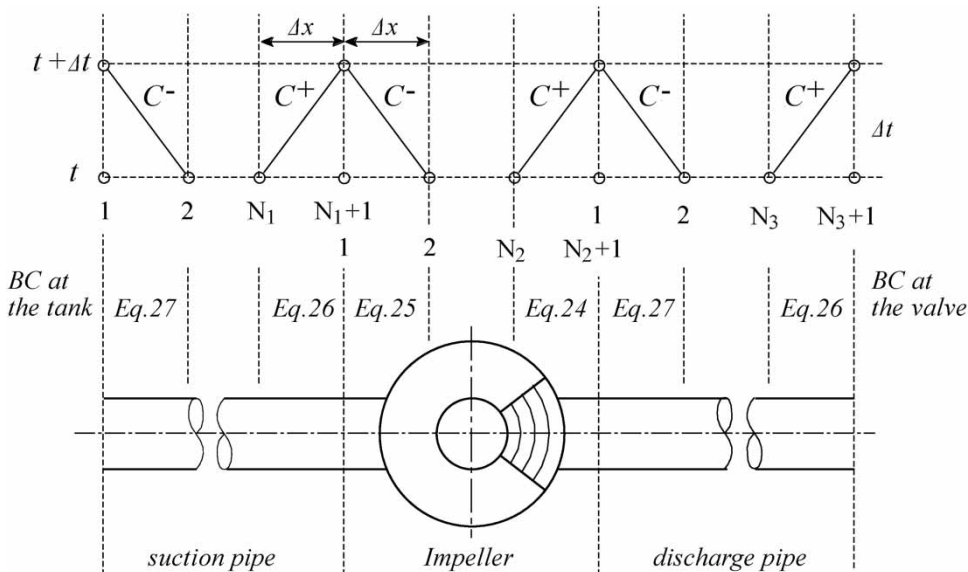

Figure 5 │ 1D model of the radial pump and boundaries conditions.

the following forms:

$$C^+ : Q_{Pi} - Q_{i-1} + \frac{gA_{i-1}}{a}(H_{Pi} - H_{i-1})$$
$$+ A_{i-1}(J_{i-1} - r_{i-1}\Omega^2)\Delta t = 0 \qquad (24)$$

$$C^- : Q_{Pi} - Q_{i+1} - \frac{gA_{i+1}}{a}(H_{Pi} - H_{i+1})$$
$$+ A_{i+1}(j_{i+1} - r_{i+1}\Omega^2)\Delta t = 0 \qquad (25)$$

Equations (24) and (25) are solved simultaneously, for each time step Δt, in order to find the unknowns H_{Pi} and Q_{Pi} in every grid point P_i. Hence, in order to get the solution until an elevated time level, it is necessary to introduce the appropriate boundary conditions (BC). The pumping system boundary conditions are presented in Figure 5, including the junctions between the pump, the suction and discharge pipe with their appropriate equations. It is also important to note that in the junction between the impeller and the volute, we have to introduce the number of the impeller vanes in the expression of the flow rate. In addition, the boundary conditions at the discharge valve are not presented herein, they can be found in Wang *et al.* (2019) and Chalghoum *et al.* (2016). Flows in the casing volute and pipes are analyzed with the same procedure without consideration of the centrifugal force term. Thus, the following equations are used:

$$C^+ : Q_{Pi} - Q_{i-1} + \frac{gA_{i-1}}{a}(H_{Pi} - H_{i-1}) + A_{i-1}J_{i-1}\Delta t = 0 \qquad (26)$$

$$C^- : Q_{Pi} - Q_{i+1} - \frac{gA_{i+1}}{a}(H_{Pi} - H_{i+1}) + A_{i+1}J_{i+1}\Delta t = 0 \qquad (27)$$

in which J is obtained from Equation (17) as:

$$J = \lambda_{vol} \frac{Q|Q|}{2gD_{hv}A_v^2} \qquad (28)$$

A numerical calculation was also introduced using Equations (10) and (11) with Equation (5) in order to determine the motor speed and torque variation, taking into consideration the friction loss of the mechanical system, the total moment of inertia and the impeller hydraulic resistant torque.

RESULTS AND DISCUSSION

We consider the experimental tests carried out by Duplaa *et al.* (2010) to verify the simulation results and validate the present numerical model. Experimental tests were carried out in the fluid Mechanics Laboratory of Lille (LMFL) with the pump fast startup test facility. The test loop is a closed circuit with the suction and delivery pipe connected to a single tank (Figure 6). In this study the close loop test facility is modeled with the 1D approach including the centrifugal pump, the induction motor, the pipes and the discharge valve, whereas experimental test conditions listed in Tables 1 and 2 are respected.

At the beginning of this simulation, the pump is started to reach its design operating point, all experimental conditions are respected and the motor pump specifications are correctly introduced. Thereafter, a fast startup simulation is carried out to analyze the motor pump transient behavior under the critical condition of quick startup.
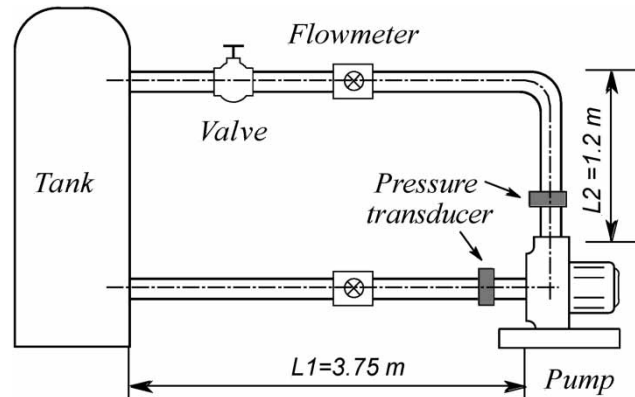

Figure 6 | Test rig scheme (Duplaa *et al.* 2010).

Table 1 | Main parameters of the impeller (Duplaa *et al.* 2010)

Impeller speed (rpm)	2,900	Inlet vane angle (deg)	32.2
Rated flow (Q_n)	23 m³/h	Outlet vane angle (deg)	23
Differential head	50 m	Number of vanes Z	5
Inlet diameter d1 (mm)	38.5	Outer width b2 (mm)	7
Outlet diameter D2 (mm)	202.5	Impeller inertia (Kg.m²)	0.0085

Table 2 | Induction motor specifications

Output power (W)	7,500	Mutual inductance M (Ohm)	0.0831
Speed (rpm)	2,875	Stator inductance L_s (Ohm)	0.0875
Stator resistance R_s (Ohm)	0.5	Rotor inductance L_r (Ohm)	0.0875
Rotor resistance R_r (Ohm)	0.85	Moment of inertia (Kg.m^2)	0.03

Subsequently, a series of simulations are reserved to study the effect of certain impeller geometric parameters on the pump transient head and the flow rate evolution.

Experimental validation

For a given rotational speed $N = 3,000$ rpm and a total inertia $I = I_m + I_p$, the pump performance curves are obtained by considering different opening positions of the discharge valve. With the change of the final flow rate, the operating point will change along the pump characteristic curves. A comparison between calculated and measured results is presented in Figure 7(a). All performance curves are in good agreement except in Figure 7(c), the shift between experiment and simulation curves is probably due to the approximation of the impeller geometry and the volute shape. To compare the
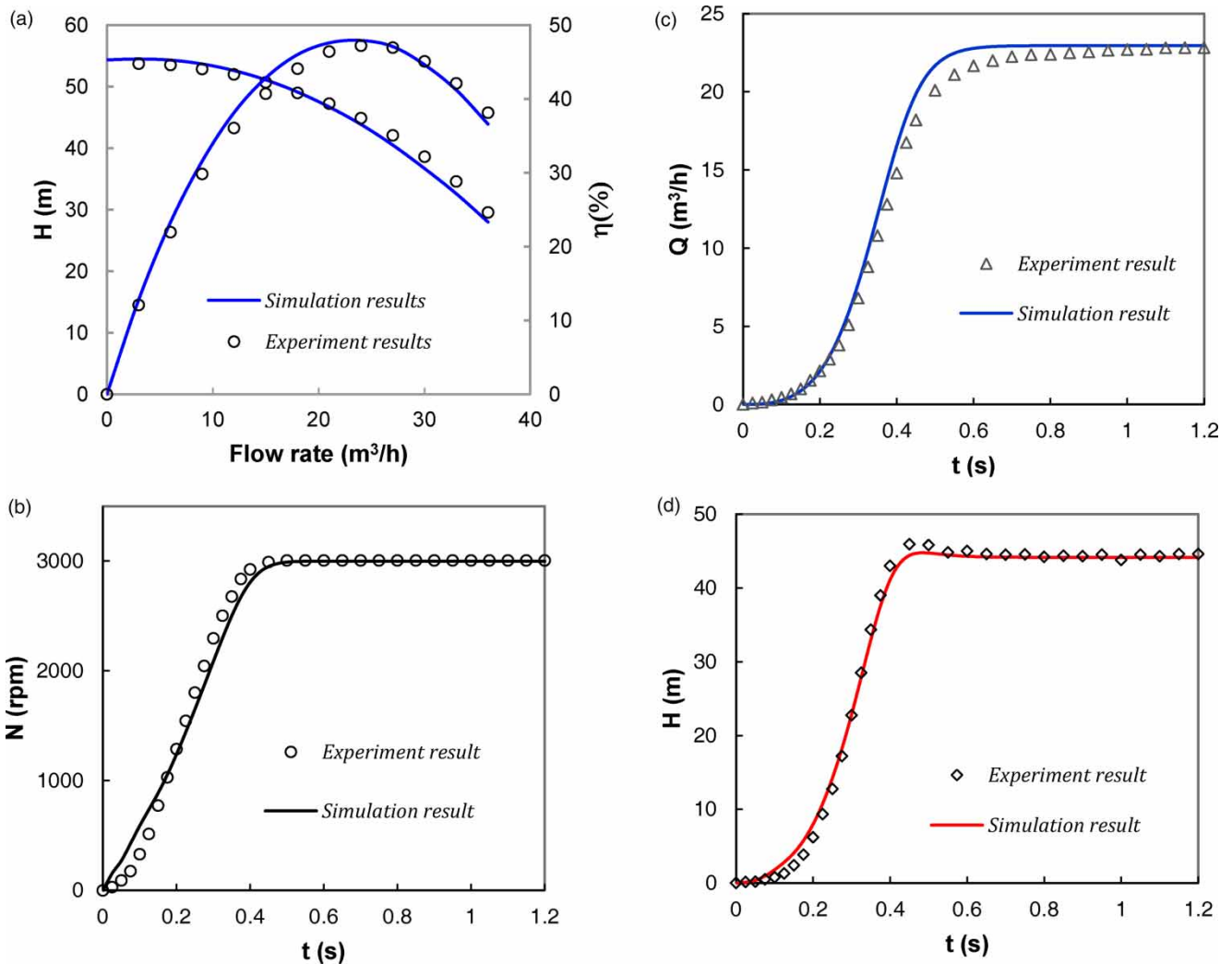

Figure 7 | Comparisons between simulated and experimental: (a) pump steady state external performances, time history of (b) impeller speed; (c) flow rate and (d) differential head during pump startup for $I = 0.065$ kg.m^2.

predicted startup characteristics with available experimental data, the impeller speed is imposed to follow the actual speed evolution and the discharge valve is adjusted to reach the nominal flow rate ($Q = 23$ m^3/h). Figure 7(b) shows a comparison between theoretical and actual impeller speed variations. Only a small shift at the beginning and the earlier step of starting time are noted. These differences are mainly due to the load torque approximation. The computed flow rate and the pump head variations are compared with experimental data and are respectively presented in Figure 7(c) and 7(d). It is also clear from Figure 7(d) that the pump head variation is in a good agreement with the experimental curve.

Fast startup simulation

To follow the actual operating conditions, a rotational speed of 2,900 rpm ($\Omega = 303$ $rads^{-1}$) is considered. The motor and pump are directly connected to the same rotating shaft. The response of the coupled system is simulated under fast startup condition. This typical simulation ($Q = Q_n$) is considered as a reference case. Figure 8(a) shows that the motor starting time is close to 0.4 s and this allows the impeller speed to rise from zero to 303 rad/s. As can be seen in Figure 8(b), the motor torque starts with high oscillations which gradually disappear after 0.2 s. The peak instantaneous torque is more than six times rated torque. Figure 8(c) shows that the peak instantaneous current
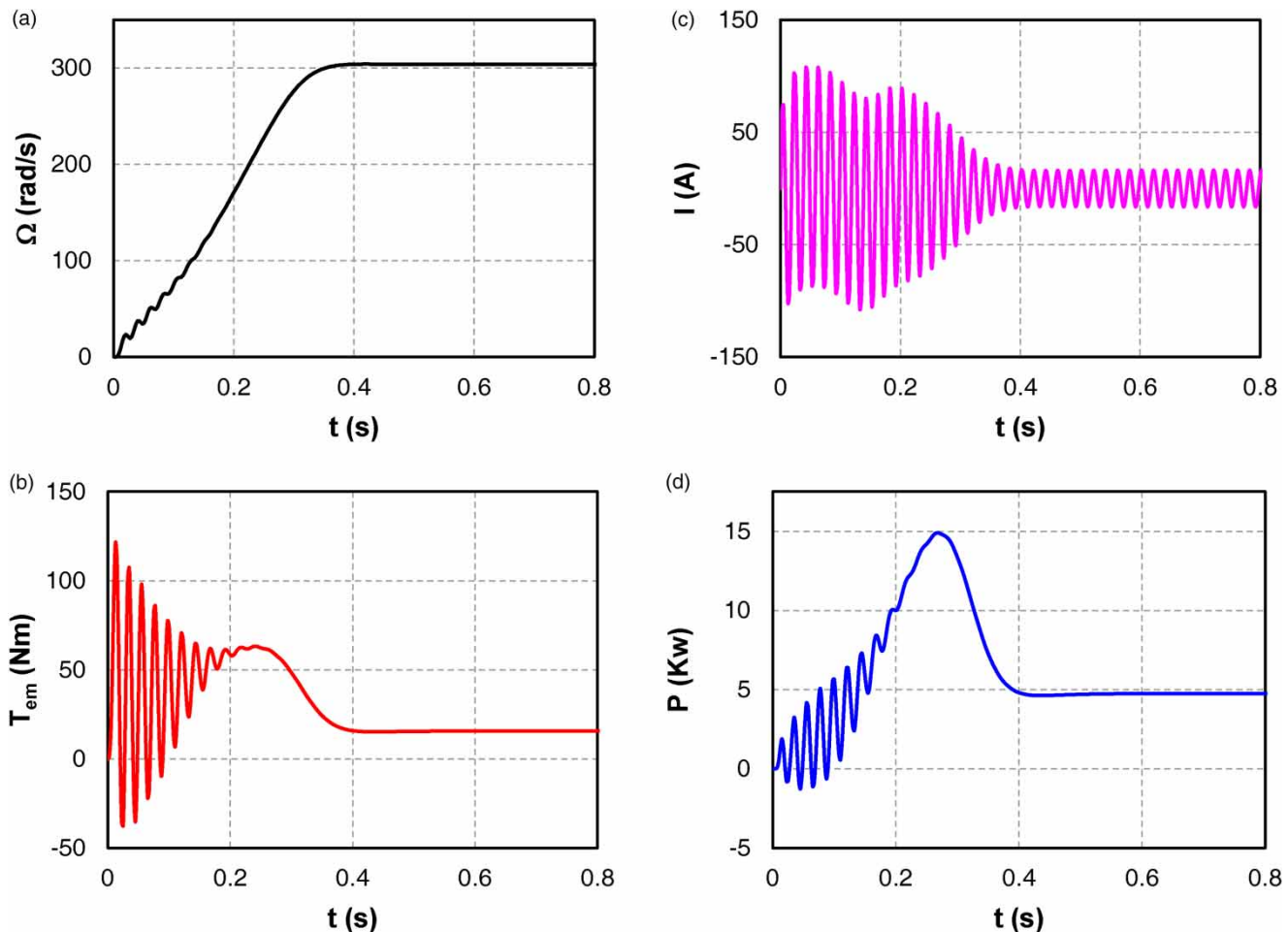

Figure 8 │ Time histories of: (a) motor speed, (b) motor torque, (c) motor stator current and (d) motor output power during pump fast startup for $I = 0.065$ kg.m^2 and $N = 2,900$ rpm.

starts at 106 A while the nominal value is only 15 A. The motor output power presented in Figure 8(d) is accompanied by significant fluctuations followed by a peak exceeding twice its rated value. Therefore, the motor torque oscillation which corresponds to the large startup current causes stator voltage drop and affects the pump dynamic responses.

The inlet, outlet and differential head variations are plotted in Figure 9(a). The outlet head rises approximately as fast as the impeller speed and it peaks before slowly stabilizing, while the inlet head goes through a negative peak exceeding cavitation limit. As presented in Figure 9(b), the pump flow rate rises gradually with a lag due to the inertial effect of the mass of water in the pump and pipes. It requires more than 0.6 s to stabilize at its nominal value. Figure 9(c) depicts the startup efficiency curve. At time $t = 0.5$ s the efficiency reaches the maximum value of 52%, while at the first stage of starting time ($t < 0.2$ s) the pump operates at almost zero efficiency.

According to Dazin *et al.* (2007), the pump transient head is mainly governed by the impeller acceleration ($\partial\Omega/\partial t$) and the flow inertia ($\partial Q/\partial t$). To focus upon this idea, the impeller speed and flow rate accelerations are plotted in Figure 9(d). The two parameters are normalized by division with their corresponding maximum value at best operating conditions and time is
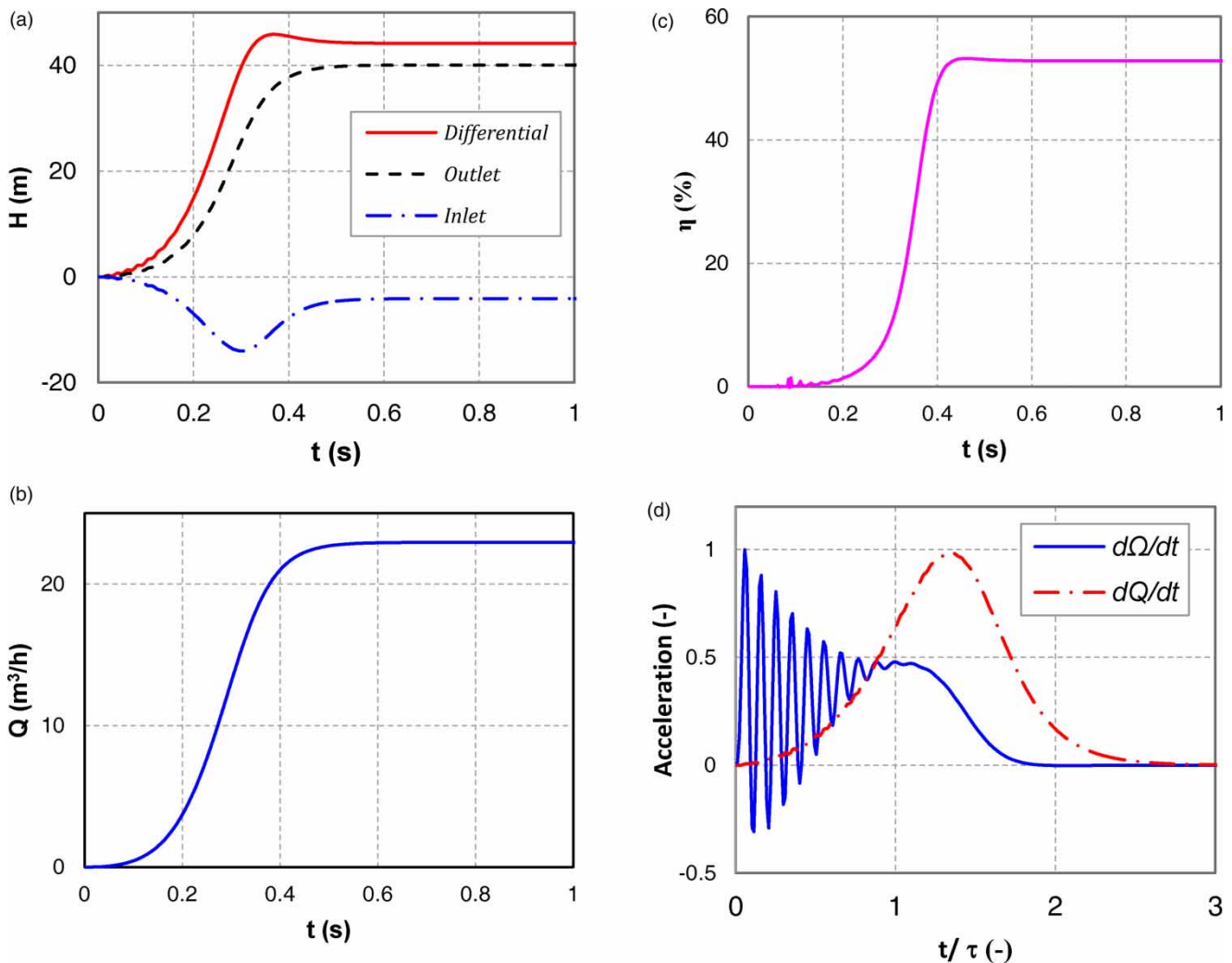

Figure 9 │ Time histories of: (a) pump head, (b) flow rate, (c) pump efficiency, (d) impeller and flow rate acceleration during pump fast startup, for $I = 0.065$ kg.m^2.

normalized by τ which corresponds to 63% of the impeller final speed. It is similar to the pump nominal acceleration time (T_{na}) used in Tsukamoto & Ohashi (1982). This coefficient is related to the motor acceleration and it is often used to characterize the pump starting time. As can be seen from Figure 9(d), during the first stage of starting time ($t - \tau$), the term $\partial\Omega/\partial t$ is dominant and it shows an oscillating profile explaining the harmful vibration induced by pump startup. Because

of the flow inertia effect, the term $\partial Q/\partial t$ is very low. Subsequently, the speed acceleration outweighs the inertial influence. Thereafter, during the second period ($\tau < t < 2\tau$), the transient flow is governed by the sum of the flow rate acceleration and impeller acceleration. Before the end of this stage, the flow inertial term becomes dominant. In the last period of starting time ($2\tau < t < 3\tau2$), the unsteady flow is only governed by the flow inertial effect.
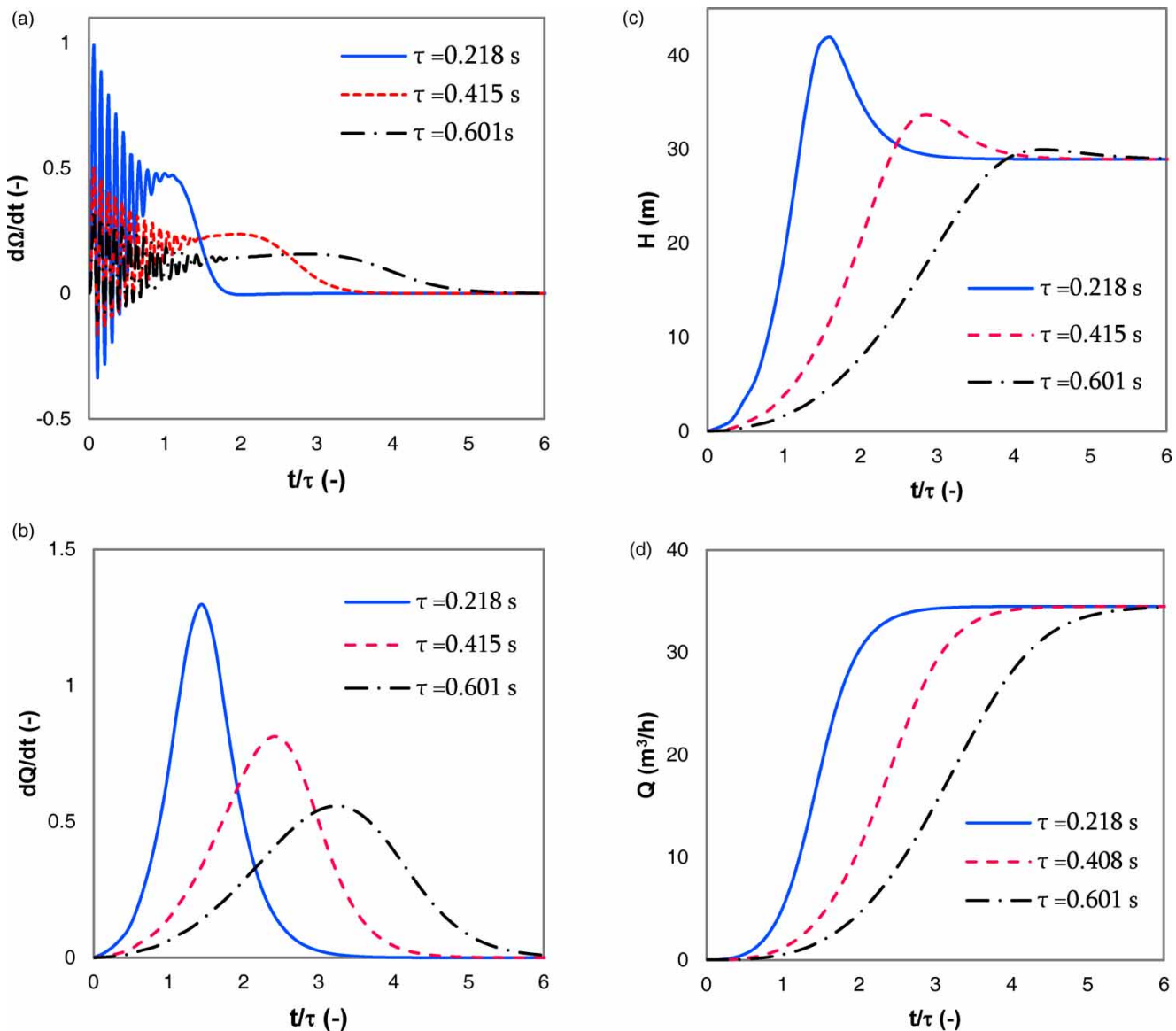

Figure 10 | Effect of τ on: (a) impeller speed acceleration, (b) flow rate acceleration, (c) pump head evolution, (d) flow rate evolution during pump startup, for $Q = 1.5\,Q_n$.

Parameters affecting the pump startup

A series of numerical simulations have been performed to investigate the effect of several parameters on the pump startup characteristics. Because of their importance in hydraulic transients, only the responses of pump head and flow rate acceleration are analyzed here.

Effect of the acceleration time and the final flow rate

The impeller acceleration is mainly affected by the mechanical inertia of the coupled rotating parts. However, it is not practically affected by the final flow rate. In Figure 10(a), the difference between the impeller acceleration curves is noticeable. For a large starting time the impeller accelerates slowly and the size of fluctuations at the first stage decrease remarkably. The same effect is seen in Figure 10(b)–10(d), low acceleration time leads to fast startup and induces a large head impact, whereas large acceleration time causes slow startup and reduces the head impact.

The effect of final flow rate on the flow acceleration and pump head variation are plotted in Figure 11. The flow rate acceleration traces a symmetric path whose delay is proportional to the final discharge (Figure 11(a)). The pump head evolution shows a significant peak before stabilizing. This impact is also proportional to the quantity of water delivered by the pump. Furthermore, as can be seen from

Figure 11(b), when the pump operates under small flow rate the pressure head increases gradually without exceeding its final value because of the reduction of the hump in flow rate acceleration.

Effect of the impeller geometry

Four important parameters are considered to analyze the effect of the impeller geometry on the pump head evolution. These parameters are the inlet diameter, blade height, blade exit angle and blade number. All simulations are carried out with the same final speed (2,900 rpm). The impeller outlet diameter (D_2) is not changed and the discharge valve is kept in the same position (full open).

The influence of the inlet diameter on the transient head evolution is evaluated in Figure 12(a). Smaller diameter ($d_1 = 40$ mm) results in the highest head impact (40.9 m), but there is no significant effect on the required starting time. Figure 12(b) presents the effect of the impeller blade height on the pump head evolution. The large head impact (49.2 m) is obtained with the highest impeller blade ($b = 12$ mm), such a pump impeller requires more time to reach its stationary regime. It is evident from Figure 12(c) that a higher blade angle (60°) leads to a larger head impact (43.15 m). Indeed, there is a decrease tendency on the required starting time with decreasing the blade exit angle. This is because of the impeller slip factor effect and
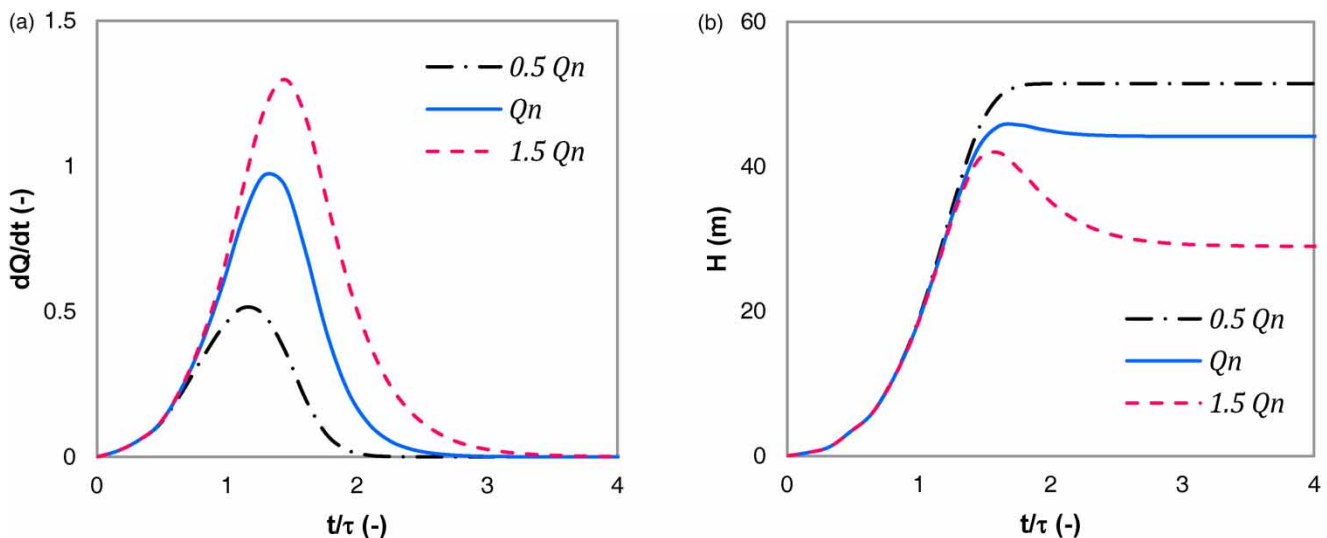

Figure 11 │ Effect of the final flow rate Q on: (a) the flow acceleration, (b) the pump head evolution for $\tau = 0.218s$.
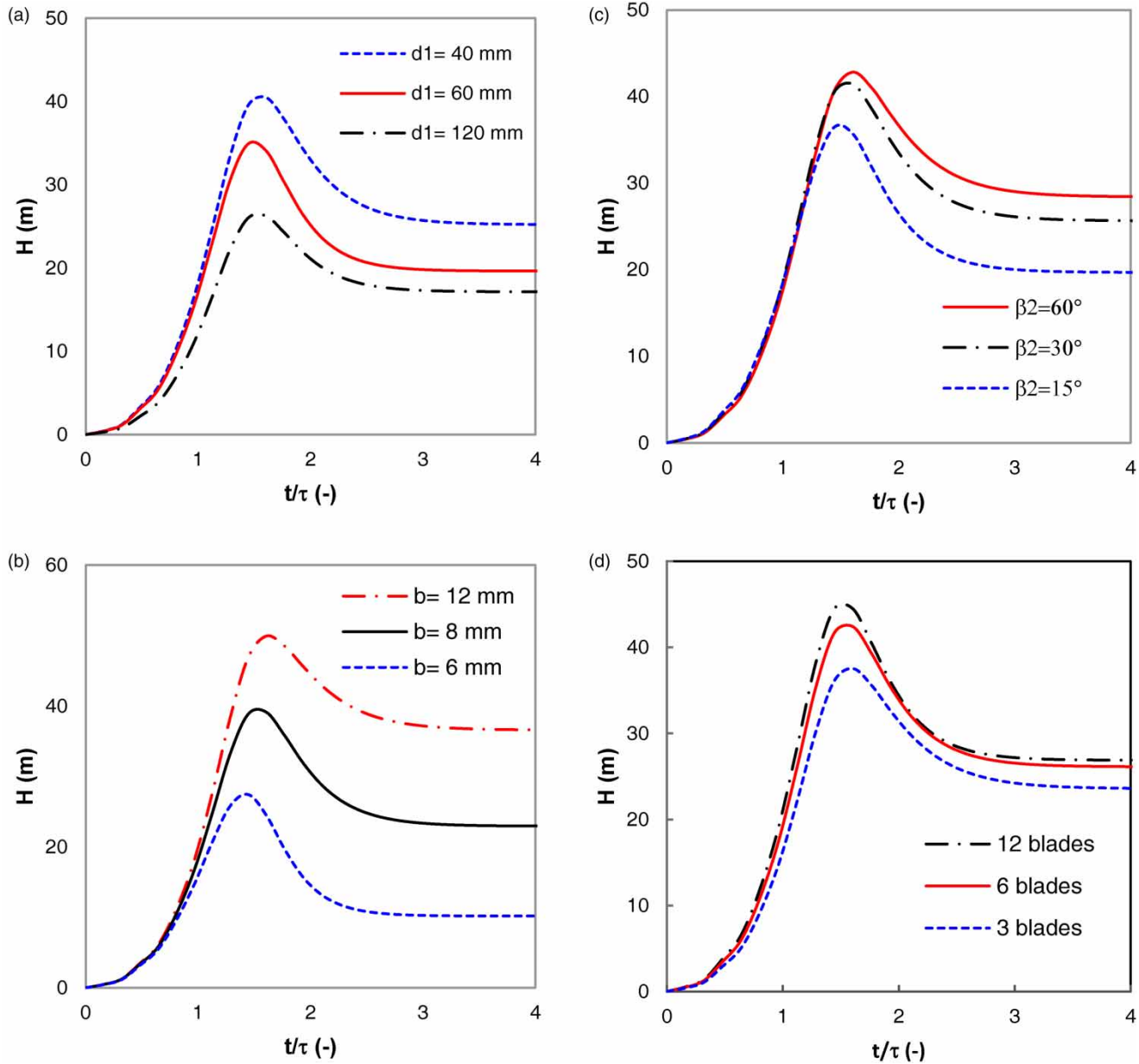
Figure 12 │ Effect of: (a) the inlet diameter, (b) the impeller blade height, (c) the blade exit angle, and (d) the blade number on the pump total head evolution during pump startup for $\tau = 0.218s$.

the transient axial thrust of the moving water. The influence of the impeller blade number (Z) on the pump transient head is plotted in Figure 12(d). The large head peak (42.8 m) is obtained with the highest blade number (12 blades), whereas the starting time tends to decrease with the impeller blade number.

Figure 13 shows the effect of four parameters of the impeller geometry on the impact head, which is defined as

the maximal difference between the suction and the delivery pressure. It is clear from Figure 13(a) that the peak head increases with decreasing the impeller inner diameter. Figure 13(b) shows that, for a given pumping system, increasing the blade height will increase the transient head impact. This is because of the large change in the mass of the moving water. It is also evident from Figure 13(c) that the peak of the transient head is proportional to the impeller
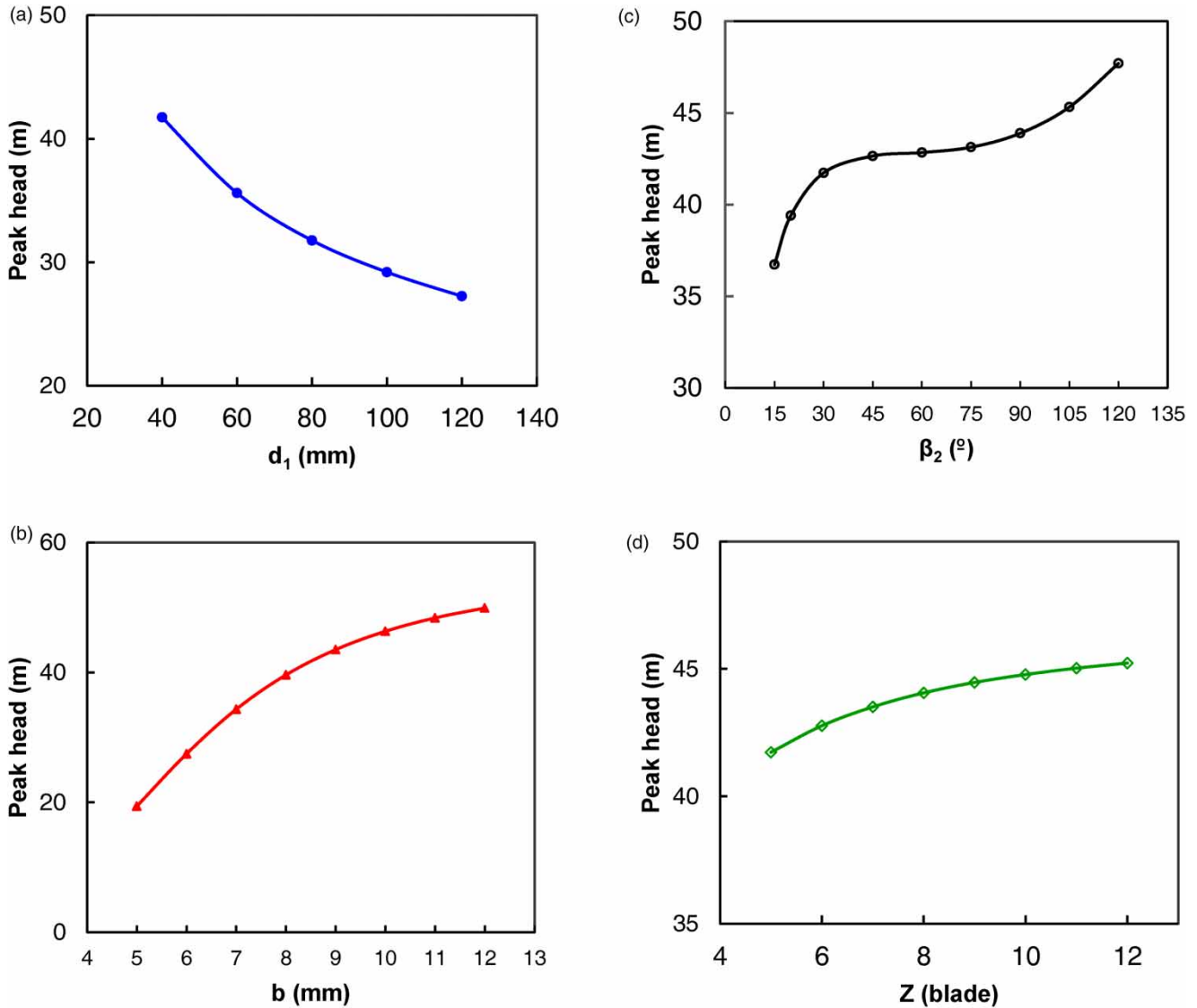
Figure 13 | Pump head impact under various: (a) inlet diameter, (b) impeller blade height, (c) blade exit angle, and (d) blade number at pump startup.

exit angle. It is finally demonstrated in Figure 13(d) that the number of the impeller blade has no important consequence for the startup head impact.

CONCLUSIONS

In this paper, the radial pump startup transients are analyzed by numerical method. The dynamic response of the coupled motor pump is investigated for different startup conditions. The predicted results have a similar trend with experimental data. Furthermore, the influence of the impeller acceleration time, final flow rate and impeller geometry on the pump transient head is studied. Through the analysis of numerical results the following conclusions are found:

- The impeller acceleration ($\partial\Omega/\partial t$) and the flow rate acceleration ($\partial Q/\partial t$) are two important parameters that can determine the pump transient head evolution.
- Fast startup causes high torque oscillations and large head impact, however, large acceleration time leads to slow startup and reduces the pressure head fluctuation.

- The transient head fluctuation shows a tendency to increase with the increase of pump final flow rate. However, when the pump operates under small flow rate, the pump head increases gradually without exceeding its final value.
- The unsteady flow in a centrifugal pump depends on its impeller geometry. A large change in the transient head curve is observed with different blade heights. The impeller blade exit angle has also a remarkable effect on the startup head evolution. Nevertheless, only a small change in the head evolution is noticed by varying the impeller blade number. In addition, the transient head impact is well influenced by the impeller inner diameter.
- With acceptable accuracy and simple implementation, the characteristic method proves its effectiveness for the approximation of flow governing equations and investigation of the transient behavior of pumping systems.

DATA AVAILABILITY STATEMENT

All relevant data are included in the paper or its Supplementary Information.

REFERENCES

Bing, H., Tan, L., Cao, S. & Lu, L. 2012 Prediction method of impeller performance and analysis of loss mechanism for mixed-flow pump. *Science China Technological Sciences* **55** (7), 1988–1998. https://doi.org/10.1007/s11431-012-4867-9.

Brennen, C. E. 1994 *Hydrodynamics of Pumps*. Oxford University Press, Oxford, UK, pp. 48–51.

Chalghoum, I., Elaoud, S., Akrout, M. & Taieb, E. H. 2016 Transient behavior of a centrifugal pump during starting period. *Applied Acoustics* **109**, 82–89. https://doi.org/10.1016/j.apacoust.2016.02.007.

Chaudhry, M. H. 1979 *Applied Hydraulic Transients*, 3rd edn. Springer, New York, https://doi.org/10.1139/l88-019

Chen, X., Zhang, J., Li, N., Yu, X., Chen, S. & Shi, L. 2021 Formula for determining the size of the air tank in the long-distance water supply system. *Journal of Water Supply: Research and Technology-Aqua* **70** (1), 30–40. https://doi.org/10.2166/aqua.2020.095.

Darweesh, M. S. 2018 Assessment of variable speed pumps in water distribution systems considering water leakage and transient operations. *Journal of Water Supply: Research and Technology-Aqua* **67** (1), 99–108. https://doi.org/10.2166/aqua.2017.086.

Dazin, A., Caignaert, G. & Bois, G. 2007 Transient behavior of turbomachineries: applications to radial flow pump startups. *Journal of Fluids Engineering, Transactions of the ASME* **129** (11), 1436–1444. https://doi.org/10.1115/1.2776963.

Duan, H.-F., Pan, B., Wang, M., Chen, L., Zheng, F. & Zhang, Y. 2020 State-of-the-art review on the transient flow modeling and utilization for urban water supply system (UWSS) management. *Journal of Water Supply: Research and Technology-Aqua* **69** (8), 858–893. https://doi.org/10.2166/aqua.2020.048.

Duplaa, S., Coutier-Delgosha, O., Dazin, A., Roussette, O., Bois, G. & Caignaert, G. 2010 Experimental study of a cavitating centrifugal pump during fast startups. *Journal of Fluids Engineering, Transactions of the ASME* **132** (2), 0213011–02130112. https://doi.org/10.1115/1.4000845.

Dutta, N., Planismy, K., Subramaniam, U., Padmanaban, S., Nielsen, J. & Blaabjerg, F. 2020 Identification of water hammering for centrifugal pump drive systems. *Applied Sciences* **10**, 2–27. https://doi.org/ 10.3390/app10082683.

Elaoud, S. & Hadj-Taïeb, E. 2011 Influence of pump starting times on transient flows in pipes. *Nuclear Engineering and Design* **241** (9), 3624–3631. https://doi.org/10.1016/j.nucengdes.2011.07.039.

Farhadi, K., Bousbia-salah, A. & D'Auria, F. 2007 A model for the analysis of pump start-up transients in Tehran Research Reactor. *Progress in Nuclear Energy* **49** (7), 499–510. https://doi.org/10.1016/j.pnucene.2007.07.006.

Iffa, R. B. & Triki, A. 2019 Assessment of inline technique-based water hammer control strategy in water supply systems. *Journal of Water Supply: Research and Technology-Aqua* **68** (7), 562–572. https://doi.org/10.2166/aqua.2017.086.

Krause, P. C., Wasynczuk, O., Sudhoff, S. & Pekarek, S. 2013 *Analysis of Electric Machinery and Drive Systems,* 3rd edn. John Wiley & Sons, Hoboken, NJ.

Lee, R. J., Pillay, P. & Harley, R. G. 1984 D, Q reference frames for the simulation of induction motors. *Electric Power Systems Research* **8** (1), 15–26. https://doi.org/10.1016/0378-7796(84)90030-0.

Li, W. G. 2011 Blade exit angle effects on performance of a standard industrial centrifugal oil pump. *Journal of Applied Fluid Mechanics* **4** (3), 105–119.

Li, Z., Wu, P., Wu, D. & Wang, L. 2011 Experimental and numerical study of transient flow in a centrifugal pump during startup. *Journal of Mechanical Science and Technology* **25** (3), 749–757. https://doi.org/10.1007/s12206-011-0107-7.

Lucius, A. & Brenner, G. 2011 Numerical simulation and evaluation of velocity fluctuations during rotating stall of a centrifugal pump. *Journal of Fluids Engineering, Transactions of the ASME* **133** (8), 1–8. https://doi.org/10.1115/1.4004636

Matteo, L., Dazin, A. & Tauveron, N. 2019 Modelling of a centrifugal pump using the CATHARE-3 one-dimensional transient rotodynamic pump model. *International Journal of*

Fluid Machinery and Systems **12** (2), 147–158. https://doi.org/10.5293/IJFMS.2019.12.2.147.

Mimouni, M. F., Mansouri, M. N., Benghanem, B. & Annabi, M. 2004 Vectorial command of an asynchronous motor fed by a photovoltaic generator. *Renewable Energy* **29** (3), 433–442. https://doi.org/10.1016/S0960-1481(03)00226-X.

Okoro, O. I. 2003 Steady state and transient analysis of induction motor driving a pump load. *Nigerian Journal of Technology* **22** (1), 46–53.

Orille, A. L., Sowilam, G. M. A. & Valencia, J. A. 1999 New simulation of symmetrical three phase induction motor under transformations of park. *Computers and Industrial Engineering* **37** (1), 359–362. https://doi.org/10.1016/S0360-8352(99)00093-5.

Page, P. R., Zulu, S. & Mothetha, M. L. 2019 Remote real-time pressure control via a variable speed pump in a specific water distribution system. *Journal of Water Supply: Research and Technology-Aqua* **68** (1), 20–28. https://doi.org/10.2166/aqua.2018.074.

Saidi, M. S. & Daneshyar, H. 1990 Unsteady one-dimensional flow with rotation. *International Journal of Mechanical Sciences* **32** (7), 581–590. https://doi.org/10.1016/0020-7403(90)90103-P.

Saito, S. 1982 The transient characteristics of a pump during start up. *Bulletin of the JSME* **25**, 372–379. https://doi.org/10.1299/jsme1958.25.372.

Thanapandi, P. & Prasad, R. 1994 A quasi-steady performance prediction model for dynamic characteristics of a volute pump. *Proceedings of the Institution of Mechanical Engineers, Part A: Journal of Power and Energy* **208** (1), 47–58. https://doi.org/10.1243/PIME_PROC_1994_208_008_02.

Thanapandi, P. & Prasad, R. 1995 Centrifugal pump transient characteristics and analysis using the method of characteristics.

International Journal of Mechanical Sciences **37** (1), 77–89. https://doi.org/10.1016/0020-7403(95)93054-A.

Triki, A. 2018 Further investigation on water-hammer control inline strategy in water-supply systems. *Journal of Water Supply: Research and Technology-Aqua* **67** (1), 30–43. https://doi.org/10.2166/aqua.2017.073.

Tsukamoto, H. & Ohashi, H. 1982 Transient characteristics of a centrifugal pump during starting period. *Journal of Fluids Engineering, Transactions of the ASME* **104** (1), 6–13. https://doi.org/10.1115/1.3240859

Wan, W. & Huang, W. 2011 Investigation on complete characteristics and hydraulic transient of centrifugal pump. *Journal of Mechanical Science and Technology* **25** (10), 2583–2590. https://doi.org/10.1007/s12206-011-0729-9

Wang, X., Zhang, J., Yu, X., Chen, S., Zhao, W. & Xu, H. 2019 Effect of multi-valve closure on superposed pressure in a tree-type long distance gravitational water supply system. *Journal of Water Supply: Research and Technology-Aqua* **68** (6), 420–430. https://doi.org/10.2166/aqua.2019.025.

Wiesner, F. J. 1967 A review of slip factors for centrifugal impellers. *Journal of Engineering for Gas Turbines and Power* **89** (4), 558–566. https://doi.org/10.1115/1.3616734.

Wu, B. Z., Xu, B. J., Li, Z. F. & Wang, L. Q. 2009 Numerical simulation on internal flow of centrifugal pump during transient operation. *Journal of Engineering Thermophysics* **30** (5), 781–783.

Wylie, E. B. & Streeter, V. L. 1978 *Fluid Transients*. McGraw-Hill International Book Co., New York, NY, USA.

Yang, S., Chen, X., Wu, D. & Yan, P. 2015 Dynamic analysis of the pump system based on MOC-CFD coupled method. *Annals of Nuclear Energy* **78**, 60–69. https://doi.org/10.1016/j.anucene.2014.12.022.